Compact, low-noise, all-solid-state laser system for stimulated Raman scattering microscopy

Tobias Steinle,[1] Vikas Kumar,[2] Andy Steinmann,[1] Marco Marangoni,[2] Giulio Cerullo,[2] and Harald Giessen[1,*]

[1]*4th Physics Institute, University of Stuttgart, Stuttgart, Germany*

[2]*IFN-CNR, Dipartimento di Fisica, Politecnico di Milano, Piazza Leonardo da Vinci 32, Milano I-20133, Italy*

**Corresponding author: h.giessen@pi4.uni-stuttgart.de*

Received October 29, 2014; revised January 7, 2015; accepted January 11, 2015;
posted January 14, 2015 (Doc. ID 225984); published February 11, 2015

We present a highly stable and compact laser source for stimulated Raman scattering (SRS) microscopy. cw-seeding of an optical parametric amplifier pumped by a bulk femtosecond Yb-oscillator and self-phase modulation in a tapered fiber allow for broad tunability without any optical or electronic synchronization. The source features noise levels of the Stokes beam close to the shot-noise limit at MHz modulation frequencies. We demonstrate the superior performance of our system by SRS imaging of micrometer-sized polymer beads. © 2015 Optical Society of America

OCIS codes: (190.5650) Raman effect; (190.7110) Ultrafast nonlinear optics.
http://dx.doi.org/10.1364/OL.40.000593

Coherent Raman scattering (CRS) microscopy is gaining increasing recognition in biomedical optics due to its capability of noninvasive, label-free imaging of tissues and cells based on their intrinsic vibrational response [1,2]. CRS microscopy also finds important applications in material science, enabling to quantify the local chemical composition and to identify nanostructures [3]. Often, CRS microscopy is used in combination with other nonlinear techniques, such as two-photon excited fluorescence (TPEF) and second-harmonic generation (SHG) microscopy, to perform multimodal imaging [4]. CRS is a class of third-order nonlinear optical techniques making use of two synchronized trains of laser pulses at frequencies ω_p (pump frequency) and ω_S (Stokes frequency). When the difference between pump and Stokes frequencies matches a characteristic vibrational frequency Ω of a molecule, i.e., $\omega_p - \omega_S = \Omega$, all the molecules in the focal volume vibrate in phase, creating a vibrational coherence which enhances the Raman response by many orders of magnitude with respect to the incoherent, spontaneous Raman process [5]. The first CRS technique to find application was coherent anti-Stokes Raman scattering (CARS) [6,7], which reads out the vibrational coherence by a further interaction with the pump beam, generating light at the anti-Stokes frequency $\omega_{aS} = 2\omega_p - \omega_S$. CARS has the advantage of being background-free, since the anti-Stokes signal can be easily isolated by spectral filtering. On the other hand, CARS suffers from the presence of the so-called nonresonant background (NRB), generated via a four-wave-mixing process and unrelated to the targeted molecular vibration. NRB distorts and sometimes overwhelms the resonant signal of interest when the concentration of the target molecules is low. Another drawback of CARS is that its signal scales quadratically with molecular concentration.

All these limitations of CARS have been overcome by the stimulated Raman scattering (SRS) technique [8,9], in which coherent interaction with the sample induces stimulated emission from a virtual state to the investigated vibrational state, resulting in a Stokes-field amplification (stimulated Raman gain, SRG) and in a simultaneous pump-field attenuation (stimulated Raman loss, SRL). SRS is inherently free from NRB and, being a self-heterodyned technique, scales linearly with sample concentration, allowing for the detection of the more dilute species and for a quantitative assessment of their concentration. Despite these important advantages, SRS is technologically more demanding than CARS, since it requires the measurement of a tiny differential signal (SRG or SRL) sitting on top of a large (and noisy) background given by the Stokes (or pump) light. Extraction of this signal requires the use of sophisticated techniques, involving high-speed modulation and lock-in detection to overcome laser fluctuations.

So far, despite their unique capabilities, practical applications of CRS techniques have been confined to high-tech research laboratories. The main stumbling block preventing widespread adoption of CRS microscopy in the biological and medical communities is the complication of the experimental apparatus. In its most widespread implementations, CRS microscopy requires the generation of two narrowband, picosecond-duration synchronized pulse trains (pump and Stokes) with tunable frequency difference, high repetition rate (≈100 MHz) and output power >100 mW per branch, in order to overcome the losses of a typical microscope. Initial CRS implementations were based on two independent picosecond Ti:sapphire lasers, tightly synchronized by a suitable electronic active control [10], resulting in a very complex, bulky, and costly set-up. A subsequent configuration, which is the current state of the art in CRS microscopy, is based on an optical parametric oscillator (OPO) pumped by a picosecond Nd:YVO_4 oscillator [11]. This system, beside its complexity, still requires cavity length synchronization between the OPO and the pump laser; in addition, the picosecond pulse duration limits the efficiency in SHG or TPEF microscopy.

Considerable effort is currently devoted to the development of compact fiber-format systems for CRS microscopy, with the aim of drastically reducing footprint and cost and increasing reliability. One architecture is based on a femtosecond Er:fiber oscillator, followed by two Er-doped fiber amplifiers, spectral broadening in highly nonlinear fibers and spectral compression via SHG, to

produce tunable pump and Stokes pulses [12–14]. This configuration has been recently upgraded by boosting the power of the Stokes arm via Yb:fiber [15] or Tm:fiber [16] amplification. An alternative scheme relies on the combination of a picosecond Yb:fiber oscillator with a fiber-based third-order optical parametric amplifier (OPA) or OPO [17–21].

Despite their clear advantages in terms of compactness and reliability, fiber lasers are difficult to apply to SRS microscopy, because they intrinsically suffer from excess high-frequency noise with respect to their bulk counterparts [15,21,22]. This is due to the much greater length of the active medium, leading to higher amplified spontaneous emission. This prevents sensitive detection of the weak nonlinear SRS signal, sitting on top of a large linear background, and requires the use of balanced detection schemes [14,15,22] with sophisticated noise-canceling electronics [15] or complex optical layouts [22].

Here we present a compact, low-cost solution for SRS/CARS microscopy, based on a bulk all-solid state Yb oscillator followed by a high repetition rate OPA. This system is simple to operate, because the high peak power of the oscillator allows to directly drive nonlinear frequency conversion processes at high repetition rates. This removes the technical complications associated with the OPO or with electronic synchronization, while at the same time preserving the unsurpassed low-noise performance of bulk solid-state systems when working with SRG detection. The outstanding stability of the Yb oscillator enables high-quality SRS imaging without balanced detection. The system also delivers femtosecond pulses for efficient multimodal imaging.

A scheme of our optical system is shown in Fig. 1. It starts with a mode-locked Yb:KGW oscillator producing 425-fs pulses at 1034 nm with 42-MHz repetition rate and 8-W average power [23]. Its rms amplitude noise is below 0.4% over 1 h. A 2-W fraction of the pulse energy is spectrally filtered by an etalon, providing a finesse of 12 and a free spectral range of 85 cm^{-1}, resulting in 1034-nm Stokes pulses with 8 cm^{-1} bandwidth and >200 mW average power. A 1.5-W fraction of the remaining power pumps a first OPA stage, based on a 10-mm-long MgO-doped periodically poled lithium niobate (PPLN) crystal and seeded by a cw laser diode generating 20 mW power at 1540 nm [24]. At this power level of the seed laser, considering the repetition rate and the pulse duration of the pump laser, the seed energy per pulse is 9 fJ, and is sufficient to largely suppress parametric superfluorescence and to overcome the energy fluctuations and timing jitter issues associated with unseeded optical parametric generation [25]. cw-seeding removes synchronization issues in the OPA and results in clean pulses with 10-nm bandwidth and 300-mW average power at 1540 nm. In the current implementation, the seed pulses are broadened by self-phase-modulation (SPM) in a tapered fiber [26] with 1.25-μm waist diameter and 8.5-cm waist length. The fiber output feeds two further OPA stages, based on 5- and 3-mm-long PPLN crystals and pumped by 1.4 and 2.5 W of the Yb:KGW oscillator, respectively, resulting in 250-fs pulses with 500–540 mW average power and tunability from 1520 to 1630 nm. The OPA, thanks to its seeded operation and multistage design allowing to work in saturation, displays good power stability, both short-term and long-term, with rms pulse-to-pulse energy fluctuations of 1.8% and average power rms fluctuations of 0.6% over 1 h [24]. Finally, SHG spectral compression [27,28] in another 20-mm-long PPLN crystal produces the 13 cm^{-1} bandwidth pump pulses, tunable from 760 to 815 nm with 4% rms pulse-to-pulse fluctuations, and allows pump-Stokes frequency detuning from 2600 to 3400 cm^{-1} with average powers in both beams of the order of 100 mW (see Fig. 2). This tuning range is fully adequate to cover the whole CH stretching region of chemical bonds, on which the vast majority of CRS applications are currently focused [1].

Note that the bandwidths of both pump and Stokes pulse can be easily adjusted to match the linewidth of the vibration of interest by selecting the etalon design and the length of the SHG crystal. Since both pump and Stokes pulses are derived from the same master Yb:KGW oscillator, they are naturally synchronized, with timing jitter negligible with respect to their duration. This considerably simplifies the setup, without the need of electronic synchronization or cavity stabilization, as in an OPO. Both pump and Stokes beam have average powers

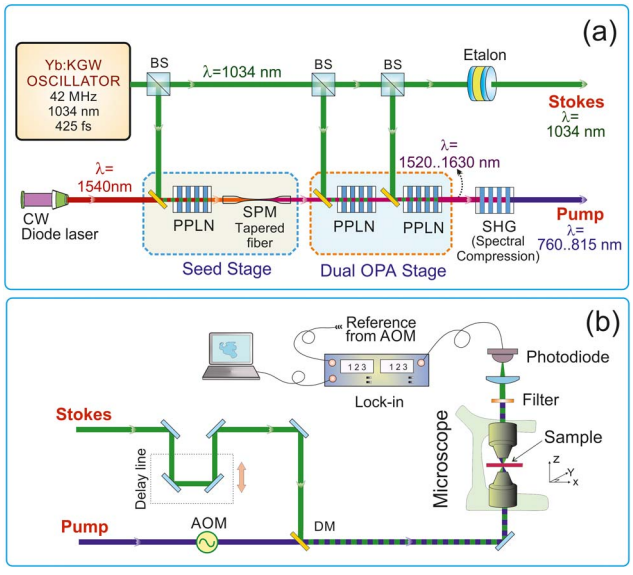

Fig. 1. Schematic diagram of the experimental system used for SRS; excitation setup (a), detection chain (b). SPM: self-phase modulation; AOM: acousto-optic modulator; BS: beam-splitter; DM: dichroic beam-splitter.

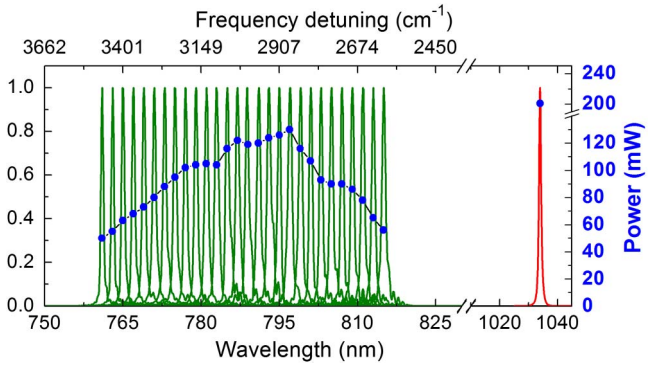

Fig. 2. Spectra of pump and Stokes pulses and corresponding average powers.

that are sufficient for SRS imaging in typical biomedical applications, taking into account the damage thresholds of cells/tissues and the typical losses of commercial microscopes. Additionally, by splitting off a fraction of the Yb:KGW output, from the OPA, or from SHG/THG beams of those, one obtains auxiliary femtosecond pulses that can be used for TPEF and SHG microscopy, thus allowing very effective multimodal imaging with our source. Such flexibility is typically not available in current SRS systems starting from picosecond oscillators.

Pump and Stokes beams are collinearly combined by a dichroic beam-splitter and sent to a homemade microscope [see Fig. 1(b)], employing two NA = 0.75 objectives. The pump beam is equipped with an acousto-optic amplitude modulator (Gooch&Housego) driven at 1-MHz frequency. The detection chain, composed of a sequence of short-pass filters, a silicon photodiode (4 MHz bandwidth), and a lock-in amplifier (Stanford Research Systems SR844), filters out the modulated pump pulses and synchronously measures the SRG of the Stokes pulses. The filter was set to 18 dB/oct. The samples are mounted on a piezo actuator (Physik Instrumente). We have chosen to modulate the pump beam and detect the SRG of the Stokes beam in order to exploit the exceptional stability of the bulk Yb:KGW laser. For this detection configuration, the noise floor of the measurement is mainly limited by the amplitude fluctuations of the Stokes beam; any contribution coming from the noisier pump pulse, which is generated by an OPA followed by nonlinear frequency conversion, is multiplied by the SRG transfer efficiency, which is typically 10^{-4} or less, and lies therefore well below the noise floor of the Stokes beam.

To estimate the sensitivity of our SRS microscope, we have measured with an electrical spectrum analyzer (Rohde&Schwarz FSL3) the relative intensity noise (RIN) spectrum of the Stokes beam, i.e., of the Yb:KGW output. The result, reported in Fig. 3, indicates that at our 1-MHz modulation frequency the RIN is −153 dB/Hz, which is within 5 dB of the shot-noise limit of −158 dB/Hz. Shot-noise-limited detection is achieved at modulation frequencies above 5 MHz. These values of RIN are significantly better than those achievable with current state-of-the-art fiber laser systems employed for SRS microscopy.

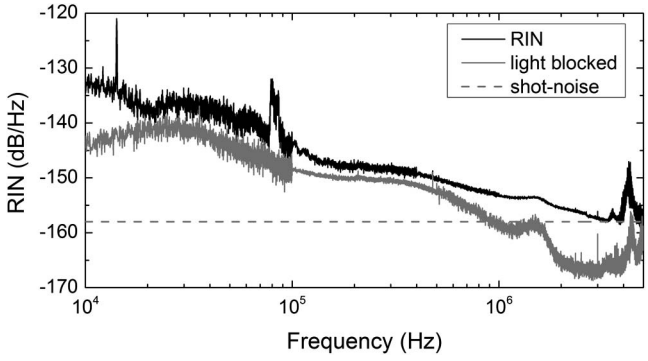

Fig. 3. RIN of the Yb:KGW pulse train. The spikes observed in the 3–5-MHz range are attributed to the electronic pre-amplifier used in the measurement. The calculated shot-noise limit is −158 dB Hz^{-1} (4 mW power incident onto the detector at 1034 nm, corresponding to the conditions used in SRS imaging).

In fact, both Freudiger *et al.* [15] and Coluccelli *et al.* [16] reported, in the 1 to 10 MHz frequency interval, RIN values that are 25–30 dB above the shot-noise limit, while in other cases the excess noise was reported to be so high to allow only CARS and not SRS imaging [21]. Close to shot-noise-limited performance can in principle be restored by balanced detection, in which a fraction of the signal beam is split off before the microscope and sent to the reference input of a balanced photodiode [14,15,22]. However, balanced detection is challenging to implement in a microscopy configuration, in which unavoidable transmission changes through the sample, since they are not experienced by the reference beam, produce unbalancing of the detector during the scan. This limitation can be overcome by the introduction of a more complicated yet effective auto-balanced detector design [15], which uses a variable gain amplifier to obtain an automatic match of reference and signal levels when scanning. Alternatively, a collinear balanced detection configuration can be used [22,29], in which both probe and reference beams, after a proper delay, are collinearly transmitted through the sample. Our system, however, achieves near shot-noise-limited performance, and allows for recording of SRS images with direct detection, avoiding all the complications of balanced detection when applied to microscopy.

To confirm the high sensitivity of our setup, we performed SRS imaging of a blend of poly-methyl methacrylate (PMMA, 6 μm diameter) and polystyrene (PS, 3 μm diameter) beads deposited on a microscope slide. Figure 4 shows raw SRG images (150 × 150 pixels) of the blend when probed at their respective Raman resonances of 2953 cm^{-1} (PMMA) and 3060 cm^{-1} (PS), with 30-ms

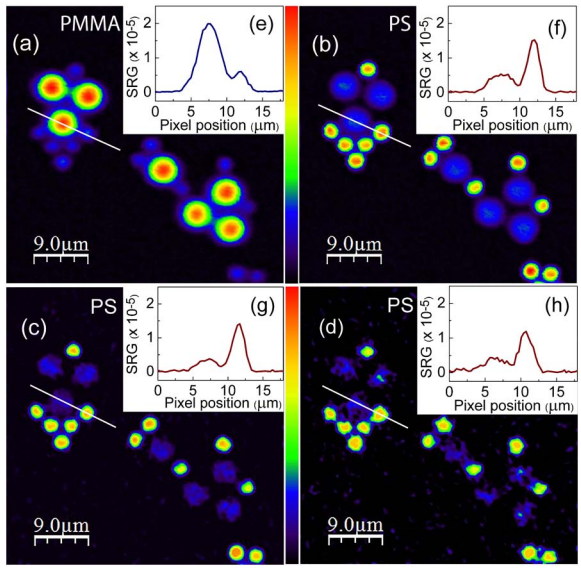

Fig. 4. (a)–(d) SRS images (150 × 150 pixels, 45 μm × 45 μm) of a blend of PMMA (6 μm) and PS (3 μm) beads when probed at their respective Raman resonances of 2953 cm^{-1} (a) and 3060 cm^{-1} (b)–(d), acquired with 30-ms (a), (b), 1-ms (c), and 100-μs (d) pixel dwell times. (e)–(h) are cross-sections of the images along the solid lines. The color scale bar ranges linearly from -0.5×10^{-6} to 2×10^{-5}. There was no background subtracted. The images show a signal-to-noise ratio of 147 (a, b), 27.7 (c), and 8.0 (d).

(a,b) or 1-ms (c) or 100-μs (d) pixel dwell time. Despite the relatively low value of the SRG ($<2\times10^{-5}$), the images are extremely clean, with signal-to-noise ratio in excess of 100 without the use of balanced detection. Considering the 3-Hz noise equivalent power bandwidth of our detection chain and the measured RIN at our 1-MHz modulation frequency, we obtain an rms fluctuation of the noise floor $<10^{-7}$, in excellent agreement with the noise values reported in Fig. 4.

In conclusion, we have presented a novel compact all-solid state system for SRS microscopy, based on a mode-locked Yb:KGW oscillator driving a cw-seeded OPA. The system is significantly simpler with respect to existing solutions based on bulk lasers, which require either electronic synchronization or cavity length stabilization of an OPO. At the same time, the system avoids the excess high-frequency noise intrinsic in fiber lasers, allowing high-quality SRS imaging without complex balanced detection schemes. Finally, it provides a synchronized femtosecond output for multimodal microscopy at different wavelengths. Currently, we used SPM in a tapered fiber to achieve full tunability over the CH stretching band. In a future upgrade, we plan to seed the first OPA stage by a tunable laser diode, covering the 1500–1630 nm range. This will avoid SPM in the tapered fiber for tuning and eliminates the need for the dual-stage amplifier, simplifying the system even further. By optimization of the laser scanner and detection chain, it should be possible to increase the acquisition speed toward video-rate imaging without complex detection electronics. Our system, when properly engineered, will significantly reduce the technical entrance barriers to SRS microscopy, bringing it closer to real-world biomedical applications in research and in therapeutics.

We would like to thank DFG, BMBF, BW-Stiftung, Carl–Zeiss–Stiftung, Alexander-von-Humboldt-Stiftung, EU-COST (MP 1302), the ERC Advanced Grant COMPLEXPLAS, and the EU Graphene Flagship (contract no. CNECT-ICT-604391) for funding.

References

1. J. P. Pezacki, J. A. Blake, D. C. Danielson, D. C. Kennedy, R. K. Lyn, and R. Singaravelu, Nat. Chem. Biol. **7**, 137 (2011).
2. A. Zumbusch, W. Langbein, and P. Borri, Progr. Lipid Res. **52**, 615 (2013).
3. A. S. Duarte, J. Rehbinder, R. R. B. Correia, M. A. Z. Vasconcellos, T. Buckup, and M. Motzkus, Nano Lett. **13**, 697 (2013).
4. S. Yue, M. N. Slipchenko, and J.-X. Cheng, Laser Photon. Rev. **5**, 496 (2011).
5. C. L. Evans and X. S. Xie, Annu. Rev. Anal. Chem. **1**, 883 (2008).
6. A. Zumbusch, G. R. Holtom, and X. S. Xie, Phys. Rev. Lett. **82**, 4142 (1999).
7. C. L. Evans, E. O. Potma, M. Puoris'haag, D. Cote, C. P. Lin, and X. S. Xie, Proc. Natl. Acad. Sci. USA **102**, 16807 (2005).
8. Ch. W. Freudiger, W. Min, B. G. Saar, S. Lu, G. R. Holtom, C. He, J. C. Tsai, J. X. Kang, and X. S. Xie, Science **322**, 1857 (2008).
9. P. Nandakumar, A. Kovalev, and A. Volkmer, New J. Phys. **11**, 033026 (2009).
10. E. O. Potma, D. J. Jones, J.-X. Cheng, X. S. Xie, and J. Ye, Opt. Lett. **27**, 1168 (2002).
11. F. Ganikhanov, S. Carrasco, X. S. Xie, M. Katz, W. Seitz, and D. Kopf, Opt. Lett. **31**, 1292 (2006).
12. G. Krauss, T. Hanke, A. Sell, D. Träutlein, A. Leitenstorfer, R. Selm, M. Winterhalder, and A. Zumbusch, Opt. Lett. **34**, 2847 (2009).
13. M. Marangoni, A. Gambetta, C. Manzoni, V. Kumar, R. Ramponi, and G. Cerullo, Opt. Lett. **34**, 3262 (2009).
14. A. Gambetta, V. Kumar, G. Grancini, D. Polli, R. Ramponi, G. Cerullo, and M. Marangoni, Opt. Lett. **35**, 226 (2010).
15. Ch. W. Freudiger, W. Yang, G. R. Holtom, N. Peyghambarian, X. S. Xie, and K. Q. Kieu, Nat. Photonics **8**, 153 (2014).
16. N. Coluccelli, V. Kumar, M. Cassinerio, G. Galzerano, M. Marangoni, and G. Cerullo, Opt. Lett. **39**, 3090 (2014).
17. M. Baumgartl, M. Chemnitz, C. Jauregui, T. Meyer, B. Dietzek, J. Popp, J. Limpert, and A. Tünnermann, Opt. Express **20**, 4484 (2012).
18. Th. Gottschall, M. Baumgartl, A. Sagnier, J. Rothhardt, C. Jauregui, J. Limpert, and A. Tünnermann, Opt. Express **20**, 12004 (2012).
19. M. Chemnitz, M. Baumgartl, T. Meyer, C. Jauregui, B. Dietzek, J. Popp, J. Limpert, and A. Tünnermann, Opt. Express **20**, 26583 (2012).
20. S. Lefrancois, D. Fu, G. R. Holtom, L. Kong, W. J. Wadsworth, P. Schneider, R. Herda, A. Zach, X. S. Xie, and F. W. Wise, Opt. Lett. **37**, 1652 (2012).
21. E. S. Lamb, S. Lefrancois, M. Ji, W. J. Wadsworth, X. S. Xie, and F. W. Wise, Opt. Lett. **38**, 4154 (2013).
22. K. Nose, Y. Ozeki, T. Kishi, K. Sumimura, N. Nishizawa, K. Fukui, Y. Kanematsu, and K. Itoh, Opt. Express **20**, 13958 (2012).
23. A. Steinmann, B. Metzger, R. Hegenbarth, and H. Giessen, *Conference on Lasers and Electro-Optics*, *OSA Technical Digest (CD)* (Optical Society of America, 2011), paper CThAA5.
24. T. Steinle, S. Kedenburg, A. Steinmann, and H. Giessen, Opt. Lett. **39**, 4851 (2014).
25. C. Manzoni, G. Cirmi, D. Brida, S. De Silvestri, and G. Cerullo, Phys. Rev. A **79**, 033818 (2009).
26. J. Teipel, K. Franke, D. Türke, F. Warken, D. Meiser, M. Leuschner, and H. Giessen, Appl. Phys. B **77**, 245 (2003).
27. M. Marangoni, D. Brida, M. Quintavalle, G. Cirmi, F. M. Pigozzo, C. Manzoni, F. Baronio, A. D. Capobianco, and G. Cerullo, Opt. Express **15**, 8884 (2007).
28. K. Moutzouris, F. Adler, F. Sotier, D. Träutlein, and A. Leitenstorfer, Opt. Lett. **31**, 1148 (2006).
29. K. Nose, T. Kishi, Y. Ozeki, Y. Kanematsu, H. Takata, K. Fukui, Y. Takai, and K. Itoh, Jpn. J. Appl. Phys. **53**, 052401 (2014).